Adaptive Impedance Matching for Magnetically Coupled Resonators

Benjamin H. Waters[1], **Alanson P. Sample**[1, 2], **and Joshua R. Smith**[1, 2]

[1]Department of Electrical Engineering, University of Washington, USA
[2]Departments of Computer Science Engineering, University of Washington, USA

Abstract— For high quality factor magnetically coupled resonator wireless power systems, constant wireless power transfer efficiency can be achieved over a greater range and higher efficiency than an inductively coupled system. However, as the distance varies between two near-field resonators, the input and output impedances to the resonators change. Therefore, in order to achieve constant efficiency, the resonator input impedance must be adaptively matched to the source impedance of the transmit resonator and the load impedance of the output device. Previous techniques have demonstrated adaptive frequency tuning control algorithms to track the resonant peaks. However, government regulations strictly limit the radiating electric field strength of wireless applications outside specific bandwidths which will be exceeded by these frequency tuning algorithms. Adaptive impedance matching (AIM) networks automatically change the input and output impedances in order to maintain maximum wireless power transfer efficiency. In this paper, the input impedance is characterized for a four-element resonant wireless power system. Two algorithms are presented to determine the component values for any adaptive impedance matching network topology to achieve constant wireless power transfer efficiency at a single frequency. These techniques are demonstrated and verified with a π-match network.

1. INTRODUCTION

Wireless power technology using magnetically coupled resonators (MCRs) is becoming more prevalent in common applications that demand efficient wireless power delivery for an entire volume of space, such as consumer electronics and implantable biomedical devices [1–6]. These applications require a highly efficient end-to-end wireless power system that can operate within the bandwidth limitations defined by wireless communication standards and regulations.

For a four-element high-Q MCR wireless power system operating in the over-coupled regime, there are two resonant modes offset by several MHz from the resonant frequency [1]. Prior work has demonstrated wideband frequency tuning techniques that automatically tune the operating frequency to maximize wireless power transfer efficiency [1, 3, 7, 8]. However, a frequency tuning algorithm used to perform maximum power point tracking may not be a viable option because the optimal operating frequency can violate the allowable frequency bandwidths where wireless power systems can operate as defined by wireless communication standards in a given country.

Rather than tuning the operating frequency to achieve maximum wireless power transfer efficiency, an impedance matching network can be used to achieve high efficiency at a single frequency within the narrow regulated bandwidth. Figure 1 shows the system-level block diagram of a wireless power system indicating an input matching network, a set of high-Q MCRs, an output matching network, a rectifier to convert the RF signal into a DC voltage compatible with a specific application, and the corresponding impedance contribution of each block. The impedance Z_{MCR} looking into the MCRs changes as a function of the mutual inductance M_{23} between the transmit (Tx) and receive (Rx) resonators. Additionally, the impedance Z_{RECT} across a full-wave rectifier changes as a function of transferred power. In order to match the varying complex system impedance $Z_{IN,SYS}$

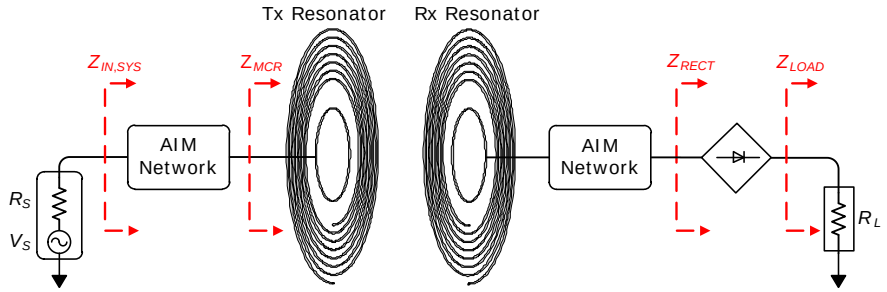

Figure 1: Block diagram of the impedance path for a high-Q MCR wireless power system.

to the source impedance R_S (typically 50 Ω from a power amplifier), an adaptive impedance matching (AIM) network can be used to induce a resonant peak at the specified operating frequency for narrowband wireless power transfer.

In this work, the impedance of each block in the wireless power system is characterized using $ABCD$ transmission matrices. Next, two separate algorithms are proposed to determine the component values of any matching network that will enable maximum wireless power transfer across a set of MCRs at a single transmit frequency. The first technique assumes an ideal matching network and directly calculates the component values of the matching network based on the input impedance Z_{MCR} extracted from measured S-parameter data for the MCRs. The second technique uses a constrained nonlinear optimization algorithm to compute the matching network component values for a lossy matching network that optimize S_{21} for a set of MCRs. Both techniques are validated using a π-match AIM network for a set of MCRs tuned to 13.56 MHz.

Although the analysis presented in this paper can be adapted to any set of MCRs, Figure 2(a) shows the set of MCRs that will be used for both the simulated and experimental inductance (L), tuning capacitance (C), and parasitic resistance (R_p) of the MCRs. These parameters are summarized in Figure 2(b). The resonators are all individually tuned for 13.56 MHz and are optimized for an optimal figure of merit (FOM) by optimizing the loop-coil coupling coefficients k_{12} and k_{34} for the best tradeoff between $|S_{21}|$ and wireless power transfer range according to [1].

2. IMPEDANCE CHARACTERIZATION OF MAGNETICALLY COUPLED RESONATORS

Before selecting an optimal matching network for MCRs, it is desirable to characterize the input impedance to a set of MCRs for a range of coupling coefficients between the resonators. The equivalent circuit diagram for a typical four-element resonant system is shown in Figure 3.

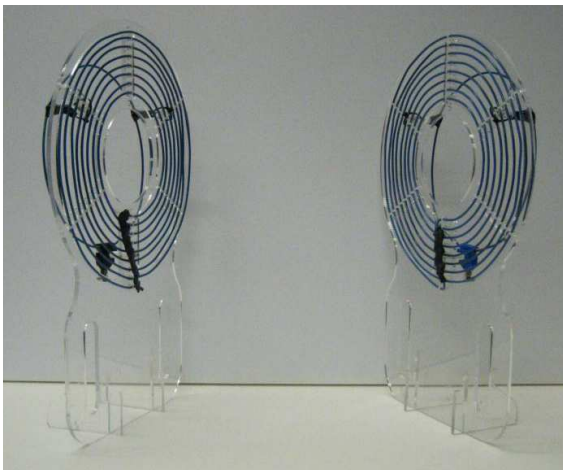

(a)

TRANSMITTER		RECEIVER	
L_1	0.6708 uH	L_4	0.6737 uH
C_1	203.19 pF	C_4	203.6 pF
R_{p1}	0.2627 Ω	R_{p4}	0.2586 Ω
N_1	1	N_4	1
Radius 1	10.25 cm	Radius 4	10.25 cm
R_{source}	50 Ω	R_{load}	50 Ω
Q_1	1.143	Q_4	1.145
F_1	13.63 MHz	F_4	13.58 MHz
K_{12}	0.2798	K_{34}	0.287
Q_2	3129	Q_3	230.29
F_{o2}	13.68 MHz	F_{o3}	13.66 MHz
L_2	17.04 uH	L_3	17.15 uH
C_2	8 pF	C_3	8 pF
R_{p2}	4.66 Ω	R_{p3}	6.36 Ω
N_2	8	N_3	8
Radius 2	14 cm	Radius 3	14 cm

(b)

Figure 2: (a) High-Q MCR resonators used throughout this work, (b) summary of coil parameter values for the MCRs.

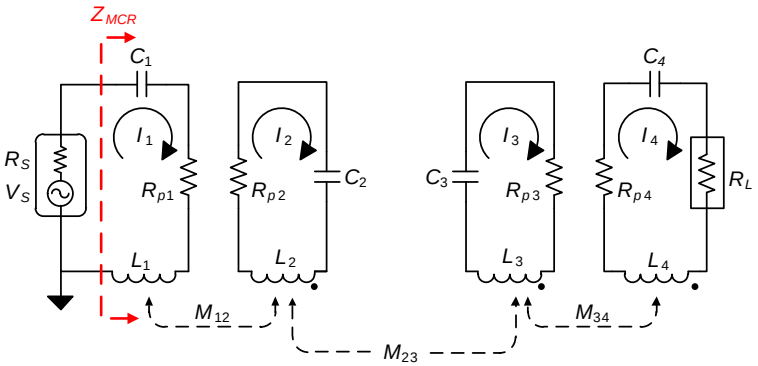

Figure 3: Equivalent circuit diagram of a 4-coil MCR wireless power system.

Flux linkages (Φ_i) and Kirchoff Voltage Loop (KVL) equations are used to solve the loop currents (I_{1-4}) indicated in Figure 3. The flux linkages across each coil are related to the voltage across the two ends of each coil. These flux linkages can also be expressed in terms of the mutual inductance (M_{ij}) between the various coils. The mutual inductance is related to the coupling coefficient k_{ij} between two inductors by (1). The current I_1 supplied by V_S flows through L_1 and produces an oscillating magnetic field. Some of these field lines pass through the other coils to produce a flux Φ_i. These flux linkages can be comprehensively expressed in terms of the mutual and self inductances for the four-element resonant system [9]. Substituting the flux linkage for each coil into the node equations derived from the four KVL equations for the schematic in Figure 3 gives (1).

$$\begin{bmatrix} V_S \\ 0 \\ 0 \\ 0 \end{bmatrix} = \begin{bmatrix} Z_1 & j\omega M_{12} & j\omega M_{13} & j\omega M_{14} \\ j\omega M_{21} & Z_2 & j\omega M_{23} & j\omega M_{24} \\ j\omega M_{31} & j\omega M_{32} & Z_3 & j\omega M_{34} \\ j\omega M_{41} & j\omega M_{42} & j\omega M_{43} & Z_4 \end{bmatrix} \begin{bmatrix} I_1 \\ I_2 \\ I_3 \\ I_4 \end{bmatrix}, \quad k_{ij} = \frac{M_{ij}}{\sqrt{L_i L_j}} \tag{1}$$

After solving for the individual currents, neglecting the parasitic cross-coupling terms ($M_{13} = M_{14} = M_{24} = 0$) and setting $M_{12} = M_{21}$, $M_{23} = M_{32}$ and $M_{34} = M_{43}$, the equivalent input impedance Z_{MCR} can be defined by (2).

$$\begin{aligned} Z_{MCR} &= \frac{V_S}{I_1} - R_S = \frac{M_{12}^2(M_{34}^2\omega^4 + \omega^2 Z_3 Z_4) - (R_S - Z_1)(M_{34}^2\omega^2 Z_2 + M_{23}^2\omega^2 Z_4 + Z_2 Z_3 Z_4)}{M_{34}^2\omega^2 Z_2 + M_{23}^2\omega^2 Z_4 + Z_2 Z_3 Z_4} \\ Z_1 &= R_S + R_{P1} + j\omega L_1 + \frac{1}{j\omega C_1} \\ Z_2 &= R_{P2} + j\omega L_2 + \frac{1}{j\omega C_2} \\ Z_3 &= R_{P3} + j\omega L_3 + \frac{1}{j\omega C_3} \\ Z_4 &= R_L + R_{P4} + j\omega L_4 + \frac{1}{j\omega C_4} \end{aligned} \tag{2}$$

Figure 4 shows the simulated Z_{MCR} plotted against k_{23} at a single frequency of 13.56 MHz for the extracted L, R, C components of the resonators shown in Figure 2. This plot indicates that for strong coupling between the two resonators (over-coupled regime [1]) $|Z_{MCR}| < R_S$ and for weak coupling (under-coupled regime) $|Z_{MCR}| > R_S$. The critical coupling point occurs when $|Z_{MCR}| = R_S = 50\,\Omega$. Therefore, an AIM network must be able to match a load impedance that can be either greater than, less than or equal to the source impedance.

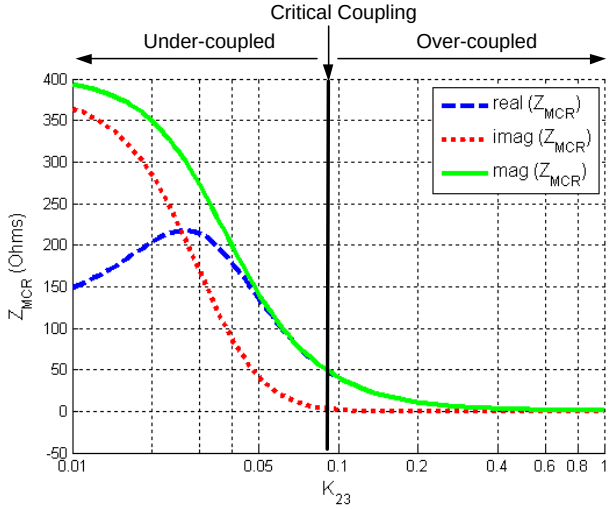

Figure 4: Plot of the real, imaginary, and magnitude components of Z_{MCR} as a function of K_{23}.

3. MATCHING NETWORK COMPONENT SELECTION

To determine the component values of any impedance matching network at a given frequency, the source and load impedances of the matching network must be accurately defined. For the resonant wireless power system shown in Figure 1, the equivalent impedance (Z) matrix can be accurately defined by analyzing each step in the impedance path as a two-port network.

The components in each block can be defined with either ideal components, lossy components, or with extracted scattering (S) parameters from a vector network analyzer (VNA) for the most accurate analysis. For example, an inductor can be modeled as either a lossless component or as a lossy component with a series DC resistance (DCR) based on the parasitic parameters provided by the manufacturer. However, the most accurate parasitic model for an inductor can be extracted by measuring the two-port S-parameters using a VNA and importing these model parameters into a simulation tool.

Similarly for the equivalent impedance of the MCRs: the input impedance for four-element MCRs can be calculated for a given coupling coefficient using (2). However, these theoretical expressions typically neglect parasitic effects such as capacitive cross-coupling and resonator detuning that can significantly reduce efficiency at the resonant frequency for a practical system. Therefore, it is most accurate to extract S-parameters from a VNA for a full range of coupling coefficients and calculate the equivalent input impedance from S_{11} as in (3). Once the impedance characteristics of each block have been defined using these techniques, the algorithms presented in this paper can be implemented to determine the necessary component values of a matching network to match the source impedance R_s to this lumped system impedance $Z_{IN,SYS}$.

$$Z_{in} = R_S \frac{1 + S_{11}(j\omega))}{1 - S_{11}(j\omega))} \tag{3}$$

Throughout this work, a low-pass π-match impedance matching network topology will be used as in Figure 5. In contrast to an L-match topology, the π-match topology enables wideband impedance matching to load impedances that are either greater than, equal to or less than the source impedance. The low-pass π-match topology allows for a fixed inductor value to be placed in the high-current path, and variable source and load capacitor values can control the impedance matching capabilities of the matching network. This switching functionality is preferable because it is easier to implement a parallel bank of switchable capacitors than inductors in series. Additionally, the quality factor (Q_m) of the π-match network provides an extra degree of freedom to achieve wideband or narrowband impedance matching. For strongly coupled MCRs, wideband impedance matching (low Q_m) is desired, but for weak coupling, narrowband impedance matching (high Q_m) is preferable. Refer to Section 4 for an extended analysis of the π-match network implented with a set of MCRs.

3.1. Ideal Conjugate Match Algorithm

Refer to the impedance path in Figure 1 as a reference for this discussion of the matrix transformations for the ideal conjugate match algorithm. For the most accurate modeling, a VNA has been used to extract the S-parameters for a set of MCRs and the rectifier. By converting the S-matrices of the MCRs and the rectifier to $ABCD$ transmission matrices, a single transmission matrix $[ABCD]_{SYS}$ can be defined for the entire system by multiplying together the cascaded $ABCD$ matrices [10, 11]. The $[ABCD]_{SYS}$ matrix is then converted back to an S-matrix from which the equivalent input impedance Z_{MCR} can be defined as in (3).

Now, the component values of the matching network can be selected. For simplicity, the impedance contribution from the rectifier has been neglected and only the real component of Z_{MCR}

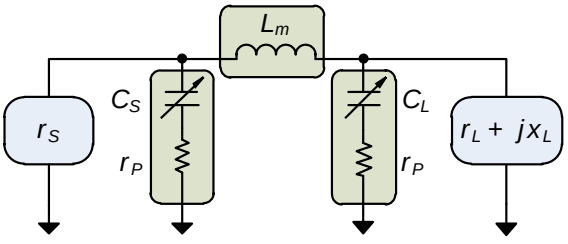

Figure 5: Block diagram of the low pass π-match network.

is used since the imaginary component of Z_{MCR} is negligible in the over-coupled regime as shown in Figure 4. The source impedance r_s seen by the π-match network is equal to R_s and the load impedance $r_l + jx_l$ is equal to $real(Z_{MCR})$. To eliminate the need for a switching circuit in the high-current path, a fixed inductor value L_m in the π-match network is chosen. The source and load capacitors (C_S and C_L) and Q_m of the π-match network can be calculated to provide an accurate impedance match for a specified source and load impedance using (4). By swapping the equations for C_S and C_L and interchanging r_s and r_l, the π-match component values can also be derived for the case when $r_s > r_l$.

$$\left.\begin{aligned} Q_m &= \sqrt{-1 + \frac{r_l(r_l + r_s)}{L_m^2 w_0^2} + \frac{2r_l\sqrt{r_l r_s - L_m^2 w_0^2}}{L_m^2 w_0^2}} \\ C_S &= \frac{\sqrt{-1 + \frac{(1+Q_m^2)r_s}{r_l}}}{r_s w_0} \\ C_L &= \frac{Q_m}{r_l w_0} \end{aligned}\right\} r_s < r_L \tag{4}$$

These expressions are used to define the component values for a π-match AIM network as Z_{MCR} changes as a function of k_{23} for a set of MCRs. From the expression for C_S, the maximum achievable quality factor ($Q_{m,\mathrm{MAX}}$) for a π-match network is determined by (5). The maximum and minimum conditions in (5) account for the additional case when $r_s > r_l$.

$$Q_{m,\mathrm{MAX}} = \sqrt{\frac{\max(r_s, r_l)}{\min(r_s, r_l)} - 1} \tag{5}$$

If Q_m exceeds $Q_{m,\mathrm{MAX}}$ for a given r_s and r_l, then C_S will not be a real number and is not achievable. Therefore, the matching network will not be able to effectively match the source impedance to the load impedance. However, L_m can be increased to reduce Q_m and ensure that the matching network can provide an optimal match for all possible values of r_s and r_l.

The advantage of implementing this algorithm in a wireless power system is that the component values of the AIM network can be directly calculated and selected by a microcontroller unit (MCU). These direct computations can be faster to perform than an optimization routine on an MCU and can be used to quickly define new component values of an AIM network for changing input and output impedances of a wireless power system.

3.2. Parasitic Match Optimization Algorithm

The second algorithm calculates the component values of non-ideal AIM networks placed at both the Tx and Rx sides of MCRs by using extracted S-parameters to define L_m and by modeling C_S and C_L with an equivalent series resistance (ESR). Rather than directly solving for the component values using the calculated source and load impedances of the matching network as in the ideal conjugate match algorithm, the parasitic match algorithm uses constrained nonlinear optimization to compute component values that maximize the magnitude of the system transmission function $S_{21,SYS}$.

By characterizing any type of impedance matching network as a two-port $ABCD$ matrix, extracted S-parameters for inductors and capacitors in the matching network can be used. In the case of the π-match network, extracted S-parameters for the series inductor can be used and converted to an $ABCD$ matrix, and the shunt source and load capacitors can be modeled with an ESR. Then, for a specified inductor, the values of $C_{S1,2}$ and $C_{L1,2}$ are optimally selected to maximize $|S_{21,SYS}|$.

The optimization routine uses the fminsearch function in Matlab. First, $S_{21,SYS}$ is defined at a single frequency as a function of $C_{S1,2}$ and $C_{L1,2}$ using the transmission matrix transformation shown in Figure 6. Next, the fminsearch function computes $C_{S1,2}$ and $C_{L1,2}$ constrained by positive real capacitor values by minimizing the error function (σ) defined in (6).

$$\sigma = \min(1 - |S_{21,SYS}|), \quad 1\,\mathrm{pF} < C_s, \quad C_L < 10\,\mathrm{nF} \tag{6}$$

There are two key benefits of this algorithm over the ideal conjugate match algorithm. First, since all components have been modeled accurately with extracted S-parameters from either the component manufacturer or a VNA, the simulated results accurately match the achievable experimental results as confirmed in Section 4. Second, it is easier than the ideal conjugate matching

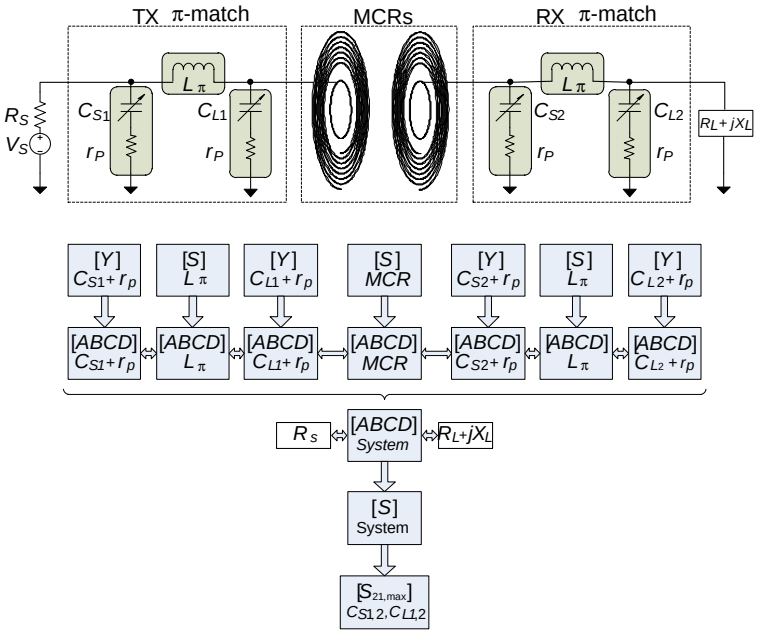

Figure 6: Flow chart of the process used for the parasitic optimization algorithm to extract the shunt capacitor values in the π-match network for an AIM network implemented with a set of high Q MCRs.

algorithm to simulate any impedance matching network topology because the equations for the components in the matching network do not need to be defined for a specific source and load impedance. Rather, the matching network can be easily defined as an $ABCD$ matrix, and after transforming the cascaded $ABCD$ matrices into a single S matrix $[S]_{System}$, the optimization algorithm automatically selects the component values for maximum $|S_{21,SYS}|$. Additionally, the matching network can be placed either at the Tx side only, Rx side only or both sides as in Figure 6 without having to re-calculate the equivalent input impedance, which becomes complicated for a double-sided matching network topology. Section 4 demonstrates that a π-match network at both the input to the Tx resonator and the output of the Rx resonator can achieve a greater $|S_{21,SYS}|$ than a matching network only at the Tx side.

4. MODEL VALIDATIONS AND EXPERIMENTAL RESULTS

A total of 87 S-parameter datasets have been extracted using a VNA for various distances between the Tx and Rx resonators shown in Figure 2(a) ranging from 0.3 cm–40 cm. These model parameters have been used to characterize the MCRs for both the ideal conjugate match and parasitic optimization algorithms presented in Section 3. A 206 nH inductor and switchable capacitors ranging from 1–1000 pF are used in the π-match AIM network. For the ideal conjugate match algorithm, both this inductor and the shunt capacitors have been modeled as ideal, lossless components. For the parasitic optimization algorithm, S-parameters provided by the manufacturer for a 206 nH air-core inductor have been used to model the inductor in the π-match network. The shunt capacitors have been modeled with a 50 mΩ ESR, a standard value for an 0603 package ceramic capacitor in the tens of MHz frequency range.

Figure 7 shows the 3D surface plots of $|S_{21,SYS}|$ versus frequency and distance between the two resonators. Figure 7(a) shows the case without an AIM network: the MCRs are terminated in 50 Ω source and load impedances. This plot demonstrates the frequency splitting effect in the overcoupled region. For a commercial application, this behavior is problematic because the efficiency at the resonant frequency of 13.56 MHz within the regulated frequency band is very low in the overcoupled regime. Figure 7(b) shows how an ideal π-match AIM network with component values selected by the simulated ideal conjugate match algorithm can confine the resonant peaks to a single ridge centered at 13.56 MHz across the entire range of separation distances. Figure 7(c) shows the effect of the simulated parasitic optimization algorithm implemented with the MCRs. For this plot, a π-match AIM network has been placed at both the Tx and Rx resonators. Although there is a significant improvement in efficiency at 13.56 MHz compared to Figure 7(a), this ridge is not as well defined as the ideal case in Figure 7(b) because parasitic components of the matching network

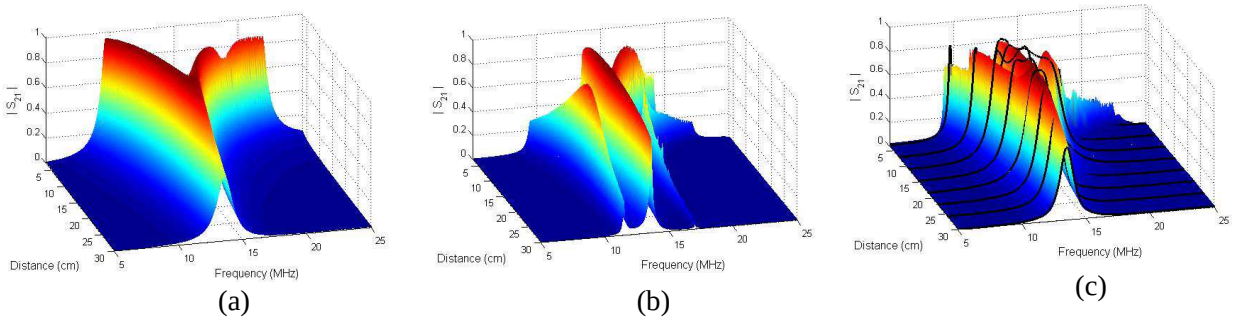

Figure 7: Surface plots of the extracted $|S_{21}|$ for the MCRs with (a) 50 Ω source and load termination impedances, (b) a π-match AIM network at the Tx side corresponding to the simulated ideal conjugate match algorithm, and (c) a π-match AIM network at both the Tx and Rx sides corresponding to the simulated parasitic optimization algorithm (surface plot) with the experimental results overlayed (black lines).

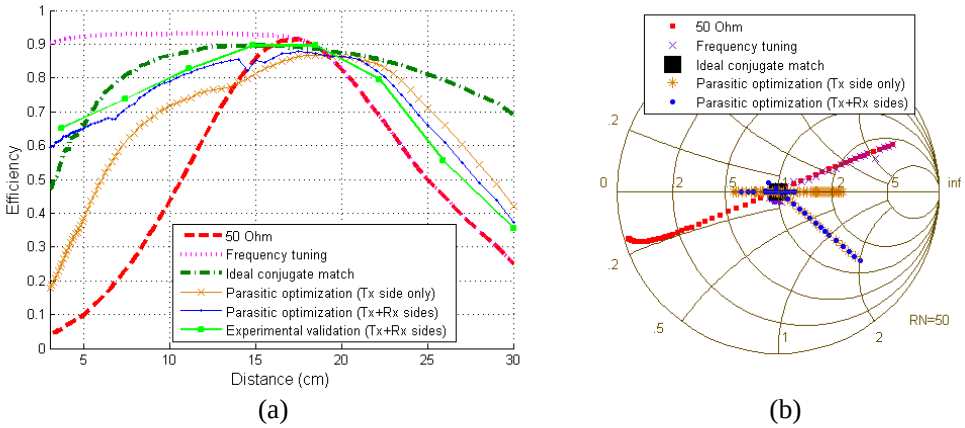

Figure 8: (a) Plot of the simulated and experimental efficiency, or $|S_{21}|^2$, and (b) a Smith chart of the simulated S_{11}.

are included in the simulation. This simulated surface plot is compared to experimental results shown by the black lines in Figure 7(c). The experimental dataset was extracted using a VNA with a π-match network on both sides for eight incremental distances between the resonators. The shunt capacitors are manually switched according to the recommended component values from the parasitic optimization algorithm. This result confirms that the simulated parasitic optimization algorithm accurately models the achievable experimental result.

Figure 8 directly compares the efficiency versus separation distance at a single frequency of 13.56 MHz for all of the simulated analyses and experimental result. Figure 8(a) includes single-frequency results for the MCRs terminated in 50 Ω, an ideal π-match AIM network at the Tx side based on the ideal conjugate match algorithm, a parasitic π-match AIM network at the Tx side as well as at both the Tx and Rx sides based on the parasitic optimization algorithm, and the experimental implementation of the double-sided parasitic optimization algorithm. Figure 8(a) also includes a result for wideband frequency tuning where the operating frequency is selected based on the maximum efficiency points along the low-frequency ridge in Figure 7(a). The AIM networks improve efficiency from the 50 Ω case at a single frequency in both the overcoupled and undercoupled regions, but cannot achieve efficiency as high as the frequency tuning results. Additionally, the S_{11} Smith chart is shown in Figure 8(b) for all of these cases. S_{11} is defined on the Smith chart at 13.56 MHz for each separation distance. The ideal conjugate match algorithm provides a perfect match to the 50 Ω source impedance at the center of the smith chart. The parasitic matching network is able to confine S_{11} towards the center, but cannot provide an accurate match for all distances.

The most problematic scenario occurs for the strongest coupling between the two resonators because the bandwidth is widest for the split resonant modes at this point. An ideal matching network is able to fully recover maximum efficiency at a single frequency for this case. However, the parasitic matching network is incapable of fully recovering maximum efficiency because the load

impedance presented to the matching network by the MCRs for strongest coupling is significantly less than the $50\,\Omega$ source impedance.

5. CONCLUSION

In this paper we demonstrate how an adaptive impedance matching network can be implemented with a set of high-Q MCRs to achieve maximum wireless power transfer efficiency at a single operating frequency. The key contributions of this work are the two algorithms presented that can compute the required component values of an AIM network for an accurate impedance match to both the input and output impedances for any amount of coupling between the MCRs.

We have characterized the input impedance for a four-element MCR system. The first algorithm uses the calculated equivalent input impedance to directly calculate the component values of a π-match AIM network. The second algorithm accounts for a non-ideal matching network by using extracted S-parameters and matrix transformations to define a system S-matrix. Then, an optimization algorithm computes the component values of a matching network that maximize the efficiency of the entire system at a single frequency. Finally, these algorithms are validated with an experimental model of the parasitic optimization algorithm.

REFERENCES

1. Sample, A. P., D. Meyer, and J. R. Smith, "Analysis, experimental results, and range adaptation of magnetically coupled resonators for wireless power transfer," *IEEE Transactions on Industrial Electronics*, Vol. 58, No. 2, 544–554, Feb. 2011.
2. Kurs, A., A. Karalis, R. Moffatt, J. D. Joannopoulos, P. Fisher, and M. Soljacic, "Wireless power transfer via strongly coupled magnetic resonances," *Science*, Vol. 317, No. 5834, 83–86, 2007.
3. Waters, B. H., A. P. Sample, P. Bonde, and J. R. Smith, "Powering a ventricular assist device (VAD) with the free-range resonant electrical energy delivery (FREE-D) system," *Proceedings of the IEEE*, Vol. 100, No. 1, 138–149, Jan. 2012.
4. Low, Z. N., R. Chinga, R. Tseng, and J. Lin, "Design and test of a high-power high-efficiency loosely coupled planar wireless power transfer system," *IEEE Transactions on Industrial Electronics*, Vol. 56, No. 5, 1801–1812, May 2009.
5. Raval, P., D. Kacprzak, and A. P. Hu, "A wireless power transfer system for low power electronics charging applications," *2011 6th Conference on Industrial Electronics and Applications*, 520–525, Jun. 2011.
6. Park, J.-H., B.-C. Park, J.-H. Lee, Y.-H. Ryu, E.-S. Park, and S.-W. Kwon, "Optimum frequency of high Q-factor resonator for magnetic resonance coupling," *2011 41st European Microwave Conference*, 61–63, Oct. 2011.
7. Kim, N. Y., K. Y. Kim, J. Choi, and C. W. Kim, "Adaptive frequency with power-level tracking system for efficient magnetic resonance wireless power transfer," *Electronics Letters*, Vol. 48, No. 8, 452–454, Apr. 2012.
8. Park, J., Y. Tak, Y. Kim, Y. Kim, and S. Nam, "Investigation of adaptive impedance matching methods for near-field wireless power transfer," *IEEE Transactions on Antennas and Propagation*, Vol. 59, No. 5, 1769–1773, May 2011.
9. Cannon, B., J. Hoburg, D. Stancil, and S. Goldstein, "Magnetic resonance coupling as a potential means for wireless power transfer to multiple small receivers," *IEEE Transactions on Power Electronics*, Vol. 24, No. 7, 1819–1825, Jul. 2009.
10. Pozar, F. M., *Microwave Engineering*, Wiley, New York, 2004.
11. Frickey, D. A., "Conversions between S, Z, Y, h, $ABCD$, and T parameters which are valid for complex source and load impedances," *IEEE Transactions on Microwave Theory and Techniques*, Vol. 42, No. 2, 205–211, Feb. 1994.